EFFECTS OF RADIATION ON THE FLAME FRONT OF HYDROGEN AIR EXPLOSIONS

A. Kessler armin.kessler@ict.fraunhofer.de
Phone +49 721 4640-301 Fax +49 721 4640-800301,
C. Wassmer, S. Knapp, V. Weiser,
K. Sachsenheimer, A. Raab, G. Langer, N. Eisenreich

Fraunhofer ICT, J.-v.-Fraunhofer Str. 7, 76327 Pfinztal, Germany

ABSTRACT

The flame velocities of unconfined gas explosions depend on the cloud size and the distance from the initiating source. The mechanisms for this effect are not fully understood; a possible explanation is turbulence generated by the propagating flame front. The molecular bands in the flame front are exposed to continuously increasing radiation intensity of water bands in the interior of the reaction product ball. A first approach to verifying this assumption is described in this paper. The flame propagation was observed by high speed video techniques including time resolved spectroscopy in the UV-Vis-NIR spectral range with a time resolution up to 3,000 spectra/s. Ignition, flame head velocity, flame contours, reacting species and temperatures were evaluated. The evaluation used video brightness subtraction and 1-dimensional image contraction to obtain traces of the movements perpendicular to the direction of propagation. Flame front velocities are found to be between 16m/s and 25 m/s. Analysis focused in particular on the flame front, which is not smooth. Salients emerge on the surface to result in the well-known cellular structures. The radiation of various bands from the fire ball on the reacting species is estimated to have an influence on the flame velocity depending on the distance from initiation. Evaluation of OH-band and water band spectra might indicate might indicate higher temperatures of the flame front induced by radiation of the fireball. But it is difficult to verify the effect relative to competing flame acceleration mechanisms.

1.0 Introduction

The flame velocities of unconfined gas explosions and those of jet fires from instantaneous sources which are moving gas explosions depend on the size and the distance from the initiating source [1-6]. Depending on the properties of releases, the mixture with air or oxygen will determine the subsequent effects. The explosive reactions occur in wide ranges of fuel/oxidizer compositions with flame velocities of more than 100m/s, which are strongly enhanced by turbulence especially in spherical explosions. The mechanisms for this effect are not fully understood, but turbulence is often assumed to be responsible, especially turbulence generated by the propagating flame front.

Hydrogen combustion in air emits radiation mainly by broad H_2O-bands in the NIR and IR spectral range and UV radiation is emitted by the dominant radical OH [7-10]. Especially in the case of large cloud explosion, the risk of heat radiation is commonly underestimated due to the non-visible flame of hydrogen-air combustion [11-13]. In realistic industrial cases explosion accidents will occur accompanied by the entrainment of contaminants of inorganic and organic substances [12, 13]. However, the flame front is composed of reacting species, mainly including OH-bands [14, 15]. These bands are exposed to the continuously increasing emission of water bands. The water bands increases until the intensity of Black Body equivalent radiation is achieved (see fig. 1). Despite cooling down the fireball, the radiation has to pass the reaction zone. Verification of this effect by experimental results, which would indicate a significant contribution to the radiation, might initiate the incorporation of radiation transport into CFD modelling. This paper describes some approach to start experimental steps for testing this assumption.

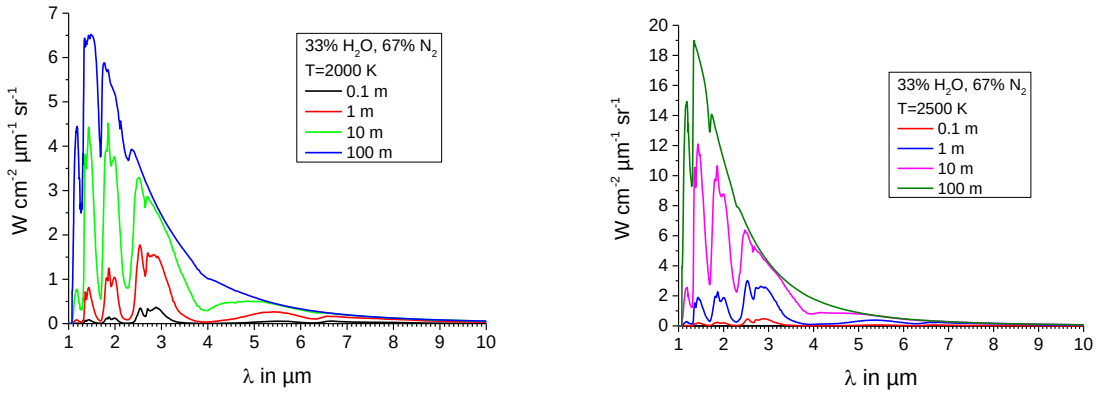

Figure 1: Radiation of the water fireball produced by hydrogen combustion. Depending on the size, the bands overlap with bands of reacting species in the flame front (taken from [9])

2.0 Experimental

The proposed effects were investigated using hydrogen air explosions with diameters up to 1m. A stoichiometric hydrogen air mixture was enclosed in a plastic foil balloon. At the start of the experiments the plastic foil was peeled off the mixture within milliseconds to generate a free cloud which was initiated in the centre by an igniter.

The flame propagation was observed by high speed video technics including time resolved spectroscopy in the UV and NIR spectral range with a time resolution up to 2000 spectra/s. Ignition, flame contours, pressure wave propagation, reacting species and temperatures were evaluated. The evaluation used brightness subtraction and 1-dimensional image contraction to obtain traces of all movements. The analysis focused in particular on the flame front perpendicular to the direction of propagation (see fig. 2) and the spots to be viewed by camera and spectrometer were selected to be at different distances from the initiation. The radiation of various water bands from the fire ball interior (fig. 1) can be absorbed by the reacting species with OH-bonds (like OH, HO_2, H_2O_2 etc. see [14, 15]) in the reaction front because of overlapping band profiles. The related energy transfer is estimated to have an influence on the flame velocity depending on the distance from initiation as bonds this radiation.

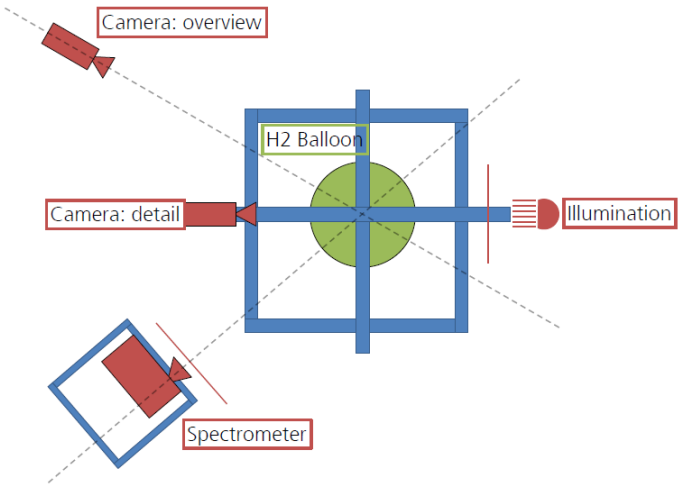

Figure 2: Schematic diagram of the experimental set-up

The camera used was a Phantom V7.1 with 800x512 pixel at 16000 fps. It recorded the transmitted light (shadow images), as shown in fig. 2.

Time resolved spectroscopy can be carried out using available equipment which consists of a fast scanning UV-spectrometer (Andor SR500i, Andor Newton DU920N-UV-BR-DD) to analyse the OH band in the spectral range of 280 to 325 nm and a NIR spectrometer (Avantes AvaSpec-NIR256) to observe the water bands between 1 and 2.3 µm. The AvaSpec-NIR256/512-2.0/2.2/2.5 Fiber Optic Spectrometers are based on the AvaBench-50 symmetrical Czerny-Turner design with 256 and 512 (2.2 model only) pixel TE Cooled extended InGaAs Detector Arrays. The spectrometer has a fibre optic entrance connector (standard SMA, other connectors also available), collimating and focusing mirror and diffractional grating. A choice of 4 gratings with different dispersion and blaze angles enables measurements in the 900-2500nm range. The AvaSpec-NIR256-2.0/2.2/2.5 instruments include a 16 bit AD converter and a USB2.0 high speed interface. The AvaSpec- NIR256/512-2.0/2.2/2.5 have a 2-stage Thermoelectrical Peltier-cooled InGaAs detector, designed for measuring in the NIR range from 1000-2000/2200/2500nm. The AvaSpec-NIR256-2.0 has a very low dark noise level enabling longer integration times for low light level applications. Analog and Digital IO ports enable external triggering and control of shuttered and pulsed light sources from the Avantes line of instruments. The AvaSpec-NIR256/512 series instruments have a USB2 interface with fast data sampling of almost 2,000 spectra per second and data transfer in 1.0 ms.

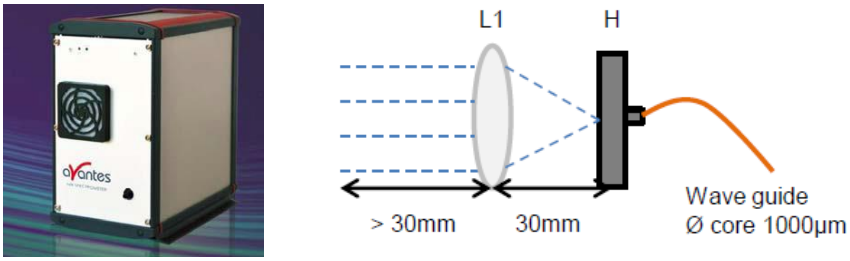

Figure 3: Avantes spectrometer to measure the water vapour bands and optics

The Andor SR500i UV/VIS-Spectrometer is an imaging spectrometer in Czerny-Turner-configuration with a focal length of 498 mm. At the exit slit of the spectrometer the Andor Newton A-DU920N-UV-BR-DD detector is adapted. The detector is a CCD (1024 x 256 Pixel with 26 x 26µm pixel size) which is a „back-illuminated“ „deep depletion“ CCD, with a special UV-coating for increased sensitivity in this wavelength range. In the “Full-Vertical-Binning-Mode” (FVB) a time resolution of 5ms/spectrum is achieved with a vertical read-out of 12.9µs (VSS = vertical shift speed) and a horizontal read-out of 1MHz (HSS = horizontal shift speed). The grating used had the following specifications: 1200 l/mm, 300 nm blaze angle, 0.027nm average resolution and 40 nm spectral range.

3.0 Results and discussion

3.1 High speed frames and evaluation

Two experiments were selected which are presented here in more detail. The spot viewed was about 8x5 cm roughly in the direction of flame propagation. A section 5.5x5cm is shown in the following figures. The flame front enters the frame section down on the right side and propagates diagonally. The initiation occurs 2cm below (fig. 4). The contrast is very low and has to be amplified. The flame front is not smooth and on propagation salients emerge as a cellular structure. Their shape might be roughly considered to be sections of spheres. This cellular structure is currently of increasing interest to understand hydrogen explosions. However, this evolving cellular structure is a competing mechanism to flame acceleration [16-19]. The research on this effect was in the past mainly related to hydrocarbon flames because the cellular structure gives an increased surface area. The visualization of the structure was carried out using the Schlieren method which limits the size to be observed.

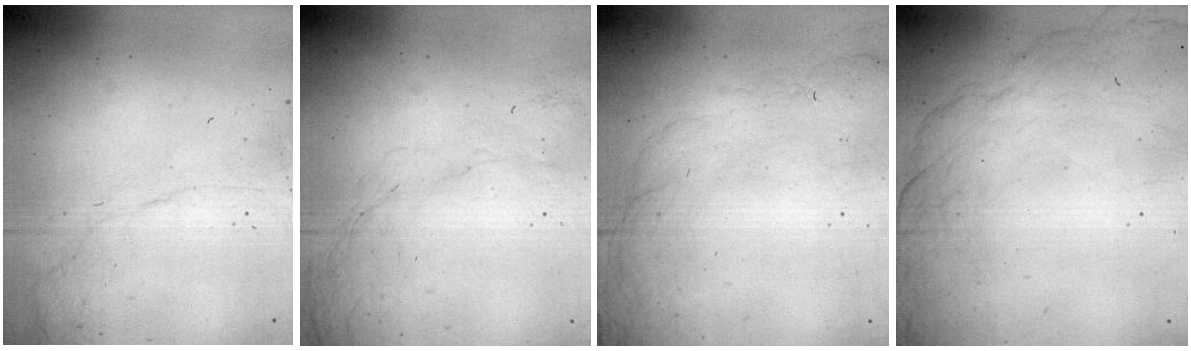

0.625ms 0.94ms 1.25ms 1.56ms

Figure 4: Flame propagation in an extracted section of 5.5cmx4.9cm (16000 fps) 2cm below ignition. The frames were reflected to be compared to the data evaluation.

The steps of image processing are shown in fig. 5: similar procedures were used to those in ref. [20, 21]. Beginning with A, the frame at 1.56ms, an edge detection was performed using a Laplacian-Gauss filter to obtain B. Then 2 adjacent frames were subtracted to obtain C [22], followed by binarization to end up at D. D shows a clear contrast and enables the further evaluation of the structures.

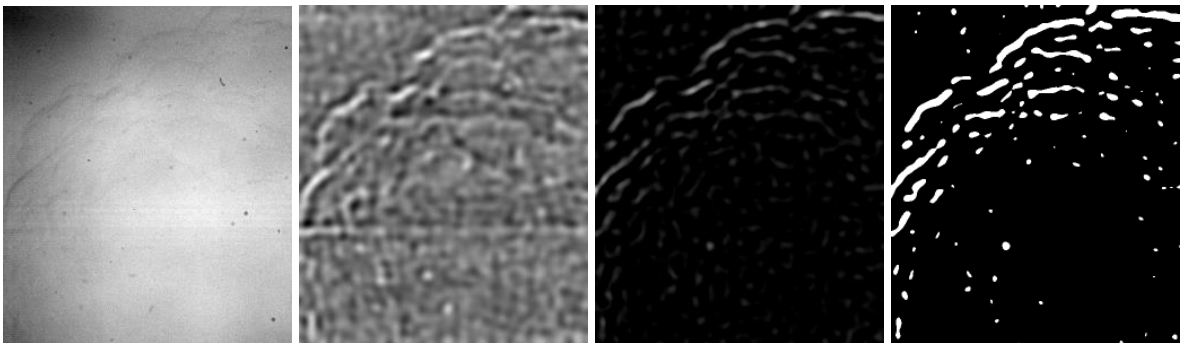

A **B** **C** **D**

Figure 5: Image processing of the frame at 1.56ms, begin: A, edge detection: B, image brightness subtraction of subsequent frames: C, binarized: D

The contour plot A in fig. 6 shows the structure close to the flame front in real dimensions. Those with a component in direction to the camera seem to be smaller. In B of fig. 6 the flame front and the salients are marked by circles. The salients are assumed to be sections of spheres with radius 15mm and with height of 3 mm in average. After emerging they retain roughly the same shape and size.

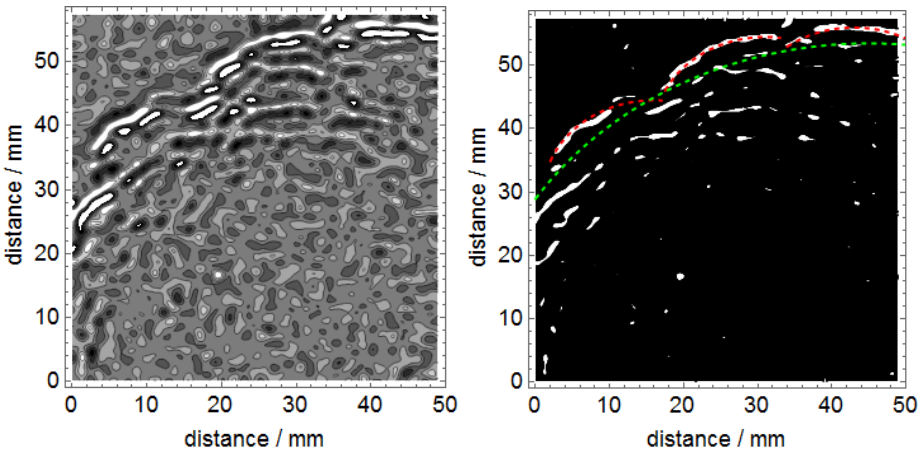

A B

Figure 6: Contour plot A and inserts of circles to mark flame front and salients.

For evaluation of the flame velocity, sections of 48mm width were extracted from the frames in direction of the flame propagation. The evaluation followed the procedures described already in earlier publications [20, 21] by image subtraction [22] and compaction of the resulting frame perpendicular to the propagation. This procedure resulted in graphs as shown in fig 8, where straight lines can be found and a fit obtained the following results: y[x]= 23.2 + 16.5 x; y1[x] = 21.75 + 15 x; the slopes give the flame velocities.

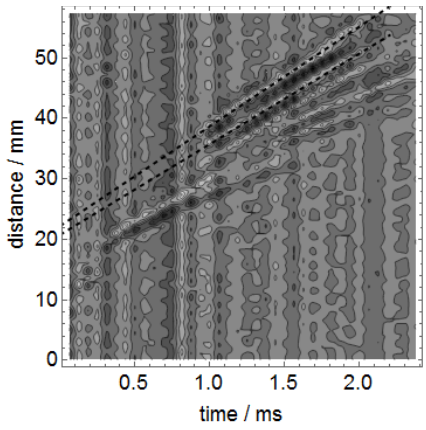

Figure 7: Contour plot of the compacted images (see [20, 21]) of the flame sections and straight lines to mark structures at the flame front

An analysis gave results for the flame front velocity (the upper line in fig. 8) of 16 to 18m/s. A slight acceleration might be identified at the end.

A further example is shown in fig. 8, with the spot of view shifted by 7.6 cm in the direction of the flame propagation.

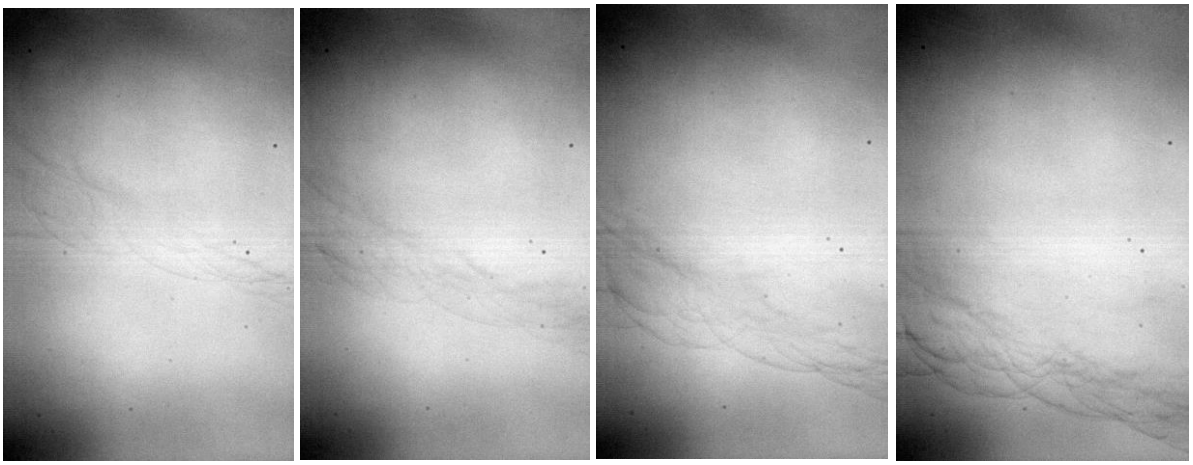

Figure 8: Flame propagation in the extracted section of 7.6cmx4.9cm, frames numbered and assigned to time when entering the section (16000 fps)

The flame front is similar to that shown in fig. 4. The salients have a similar shape and size as in the experiment described above. Fig. 9 shows one flame velocity evaluation with a straight line resulting in a velocity of 24.5m/s: y[x] = 2.8 + 24.5 x; y1[x] = -1.5 + 24.75 x. Further evaluations gave results between 23 and 25m/s.

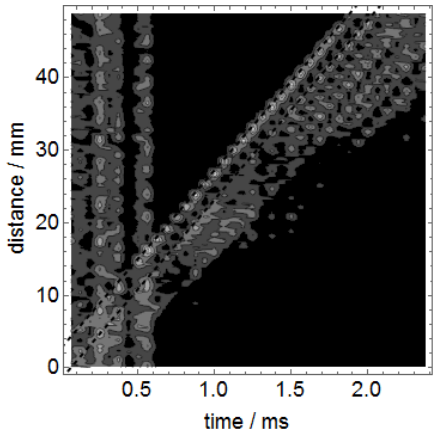

Figure 9: Contour plot of the compacted images of the flame sections and straight lines to mark structures at the flame front

3.2 Spectroscopy

UV spectroscopy acquires the OH band, at 306 - 315nm a rotational band from the 0-0 electronic/vibration transition. An example is plotted in fig.10. In gas explosions, this band tends to self-absorption which is difficult to take into account. However, a least squares fit of modelled spectra to the measured spectra were performed with the temperature as a fit parameter. The results are shown in fig. 11. The time resolution of 10ms is not adequate to resolve the reaction zone in sufficient detail. However, the results give some hints to the occurring reactions. The temperatures at the trigger, when the flame front matched the point of view, are even higher than the adiabatic flame temperature; a result often obtained for this band because of energy uptake from the reaction. However, the temperatures obtained are at least in relative agreement. The temperatures increase with increasing distance (8cm to 30cm) from the point of ignition. These results might confirm the assumption of radiation interaction of the flame front species with radiation emitted by the fireball interior.

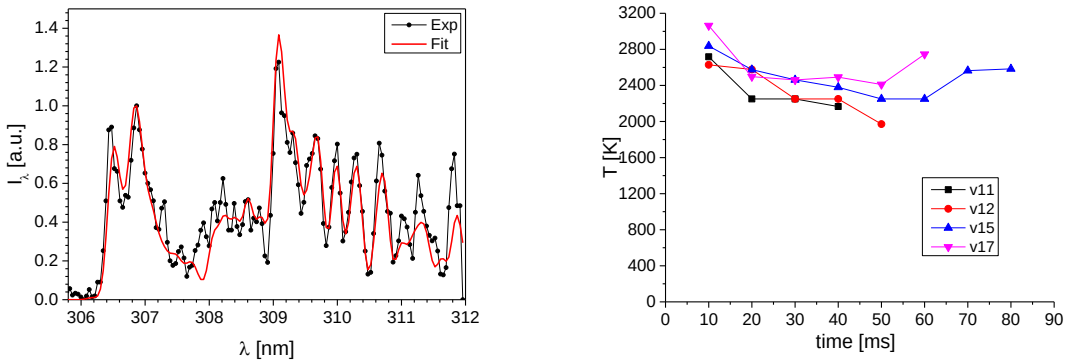

Figure 10: An example of an OH 0-0 band (left) and its fit and the resulting temperatures (right), the spectra recorded at 100/s. (v11, v12 are 8cm and v15 and v17 are 23cm from ignition)

The NIR spectra are recorded with time intervals of 0.57ms and an exposure time of 0.03ms, which are much more appropriate to the flame front resolution in time. As already found in the high speed frames, the explosion emits no continuums radiation at all, as shown in fig. 11. The strong bands occur in the NIR, as already obvious in Fig.1. Using the evaluation by the BaM code of ICT [23-25] the temperatures are between 2150 and 2250K, which is reasonable for such experiments, and they are higher than for jets with turbulent air entrainment [23, 24]. At the flame front they seem to be higher than within the time where the main emission comes from the fireball interior, but still with the flame front out of focus. The temperatures also seem to be higher for a distance of 15cm than those found at shorter distances (fig. 11).

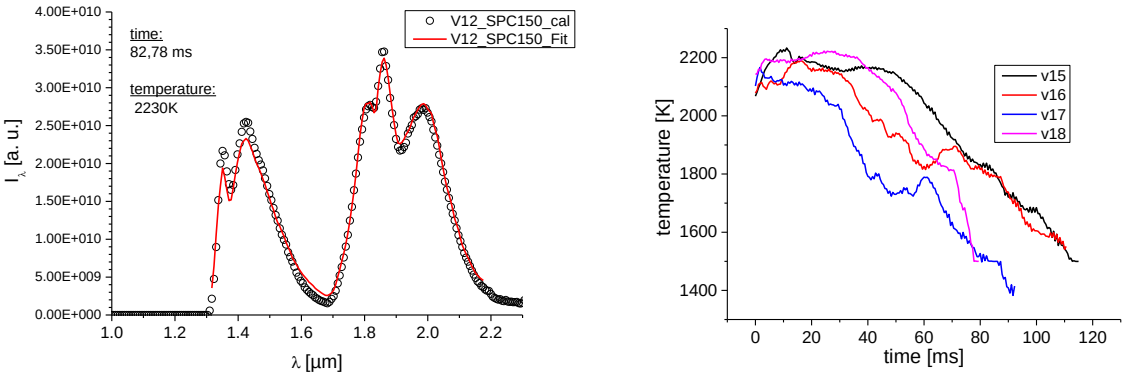

Figure 11: An example of the NIR water bands above 1.2µm (left) and their fit [] and the resulting temperature (right), for spectra recorded at 0.55 1/ms.

However, further investigations will be required for a convincing verification of this hypothesis, to acquire more details about the flame front. Such experiments are planned for the future. The results should also be discussed with relation to competing mechanisms like the cellular structure.

4.0 Conclusions

The investigations of stoichiometric hydrogen air explosions up to diameters of 1m show a cellular structure at the flame front, which is generated by emerging salients. Shape and size are similar for all experiments. Time resolved temperature measurement gives values of over 2500K for the OH rotational bands, which are often found for OH bands in a reaction zone. The temperature obtained from the water bands within the spectral interval of 1.2 and 2.2µm are more realistic in the range of 2150-2250K. They are obtained with integration times of 30µs and rates of 0.57ms. Although some evidence supports the suggestion of higher temperature depending on the distance from the point of ignition, further experiments will be required to verify this hypothesis in a convincing way.

References

1. A. Kotchourko, D. Baraldi, P. Bénard, N. Eisenreich, T. Jordan, J. Keller, A. Kessler, J. Lachance, V. Molkov, M. Steen, A. Tchouvelev, J. Wen, State of the art and research priorities in hydrogen safety, Luxembourg: Publications Office of the European Union, 2014, ISBN 978-92-79-34719-1, doi: 10.2790/99638
2. Dorofeev, S.B., Blast effects of confined and unconfined explosions, Proc. of 20th Symp. (Int.) on Shock Waves (Pasadena, CA, USA, July 1995), pp. 77-86.
3. Dorofeev, S.B., Efimenko, A.A., Kotchurko, A.S., and Chaivanov, B.B., Evaluation of the hydrogen explosions hazard, *Nuclear Engineering Design*, 148 (1995) 305-316.
4. Dorofeev, S.B., Kuznetsov, M.S., Alekseev, V.I., Efimenko, A.A., Breitung, W., Evaluation of limits for effective flame acceleration in hydrogen mixtures, *J. Loss Prev. Process Industries*, 14 , 2001, pp. 583–589.
5. Dorofeev, S.B., Sidorov, V.P. Kuznetsov, M.S., Matsukov, I.D., Alekseev, V.I., Effect of scale on the onset of detonations, *Shock Waves*, 10 (2), 2000, pp. 137-149.
6. Kuznetsov, M., Grune, J., Friedrich, A., Sempert, K., Breitung, W., and Jordan, T., Hydrogen-Air Deflagrations and Detonations in a Semi-Confined Flat Layer, In: Fire and Explosion Hazards, Proceeding 6th Int. Seminar (Ed. Bradley, D., Makhviladze, G., and Molkov, V.), 2011, pp 125-136, ISBN: 978-981-08-7724-8.
7. Gore J., Jeng S., Faeth G., Spectral and total radiation properties of turbulent hydrogen/air diffusion flames, *J. Heat. Trans.*, 109, 1987, pp165–171.

8. Kounalakis M. E, Gore J.P., Faeth G. M., Turbulence/radiation interactions in nonpremixed hydrogen/air flames, Twenty-Second Symposium (International) on Combustion, Seattle, WA. USA, August 14-19, 1988
9. Weiser V., Roth E., Kelzenberg S., Eckl W., Eisenreich N., Langer G., Measuring and modelling unsteady radiation of hydrogen combustion. 1st Int. Conf. Hydrogen Safety, Pisa, Italy, 8-10 September 2005
10. Kessler A., Schreiber A., Deimling L., Weiser V., Klan T., Billeb G., Knapp S., Eisenreich N., Radiation from Hydrogen Jet Fires Investigated by Time-Resolved Spectroscopy, paper 103, 5th Int. Conf. Hydrogen Safety, Brussels, Belgium, September 9-11, 2013
11. Houf, W. G., Schefer, R. W. Predicting radiative heat fluxes and flammability envelopes from unintended releases of hydrogen. *Int. J. Hydrogen Energy*, 32, 2007, pp. 136-151
12. Pehr K., Aspects of Safety and Acceptance of LH2 Tank Systems in Passenger Cars, *Int. J. Hydrogen Energy*, 21, 1996, pp. 387 - 395.
13. Eckl, W., Eisenreich, N., Herrmann, M.M., Weindel, M., Emission of radiation from liquefied hydrogen explosions, *Chem. Ing. Tech.*, 67, 1995, pp. 1015-17.
14. Warnatz, J. , Concentration-, pressure-, and temperature-dependence of the flame velocity in hydrogen-oxygen-nitrogen mixtures, *Combustion Science and Technology*, 26,1981, pp. 203-213.
15. Westbrook, C. K., Mizobuchi, Y., Poinsot, T. J., Smith, P. J., & Warnatz, J., Computational combustion. Proceedings of the Combustion Institute, 30, 2005, pp. 125-157.
16. Katsumi T., Kobayashi H., Aida T., Kadowak S., Propagation Characteristics of Hydrogen-Air Deflagration in a Closed Vessel, Flame Structure 2014, Berlin Sept. 2014, http://www.flame-structure-2014.com.
17. Wu, F., Jomaas, G., & Law, C. K., On Self-Acceleration of Cellular Spherical Flames, Fall Technical Meeting of the Eastern States Section of the Combustion Institute, Hosted by the University of Connecticut, Storrs, CT, Oct 9-12, 2011
18. Sun, Z. Y., Liu, F. S., Bao, X. C., & Liu, X. H., Research on cellular instabilities in outwardly propagating spherical hydrogen-air flames, *Int. J. Hydrogen Energy*, 37, 2012, pp. 7889-7899.
19. Wu, F., Jomaas, G., & Law, C. K., An experimental investigation on self-acceleration of cellular spherical flame, *Proceedings of the Combustion Institute*, 34, 2013, pp. 937-945.
20. Deimling L., Weiser V., Blanc A., Eisenreich N., Billeb G., Kessler A., Visualisation of jet fires from hydrogen release, *Int. J. Hydrogen Energy*, 36, 2011, pp. 2360-2366.
21. Schreiber A., Wassmer C., Kessler A., Deimling L., Knapp S., Weiser V., Sachsenheimer K., Langer G., Eisenreich N. Ignition of hydrogen jet fires from high pressure storage, *Int. J. Hydrogen Energy*, 39, 2014, pp. 20554–20559.
22. Otsuka T., Saitoh H., Mizutani T., Morimoto K., Yoshikawa N., Hazard evaluation of hydrogen-air deflagrations with flame propagation velocity measurement by image velocimetry using brightness subtraction, *J. Loss Prevention*, 20 ,2007, pp. 427-432.
23. Blanc A., Deimling L., Eisenreich N., Langer G., Kessler A., Weiser V., Evaluation of optical and spectroscopic experiments of hydrogen jet fires, 3rd Int. Conf. Hydrogen Safety, paper 228, Ajaccio, Corsica on September 16-18, 2009
24. Kessler A., Schreiber A., Deimling L., Weiser V., Klahn T., Billeb G., Knapp S., Eisenreich N., Radiation from Hydrogen Jet Fires Investigated by Time-Resolved Spectroscopy, paper 104, 5th Int. Conf. Hydrogen Safety, Brussels, Belgium, September 9-11, 2013
25. Weiser V., Eisenreich N., Fast emission spectroscopy for a better understanding of pyrotechnic combustion behavior, *Propellants, Explos., Pyrotechnics*, 30, 2005, pp.67-78